Microbial narrow-escape is facilitated by wall interactions

Mathieu Souzy, Antoine Allard, Jean-François Louf, Matteo Contino, Idan Tuval, Marco Polin

HAL Id: hal-04166335
https://hal.inrae.fr/hal-04166335

Submitted on 19 Jul 2023

Microbial narrow-escape is facilitated by wall interactions

Mathieu Souzy [1,*], Antoine Allard [2,*], Jean-François Louf [3], Matteo Contino,[2] Idan Tuval,[4,5,†] and Marco Polin [2,4,5,‡]

[1]*Physics of Fluids, University of Twente, P.O. Box 217, 7500AE Enschede, The Netherlands*
[2]*Department of Physics, University of Warwick, Gibbet Hill Road, Coventry CV4 7AL, United Kingdom*
[3]*Department of Chemical Engineering, Auburn University, Auburn, Alabama 36849, USA*
[4]*Mediterranean Institute for Advanced Studies, IMEDEA, UIB-CSIC, Esporles 07190, Spain*
[5]*Physics Department, Universitat de les Illes Balears, Palma de Mallorca 07122, Spain*

Cells have evolved efficient strategies to probe their surroundings and navigate through complex environments. From metastatic spread in the body to swimming cells in porous materials, escape through narrow constrictions—a key component of any structured environment connecting isolated microdomains—is one ubiquitous and crucial aspect of cell exploration. Here, using the model microalgae *Chlamydomonas reinhardtii*, we combine experiments and simulations to achieve a tractable realization of the classical Brownian narrow-escape problem in the context of active confined matter. Our results differ from those expected for Brownian particles or leaking chaotic billiards and demonstrate that cell-wall interactions substantially modify escape rates and, under generic conditions, expedite spread dynamics.

From cytoskeletal dynamics and bacterial swarming to flocks of birds and human crowds, collections of interacting self-propelling agents can display unexpected emergent properties as a consequence of being far from equilibrium. Understanding these within the framework of a general theory is a challenge which is currently driving the rapidly growing area of active matter physics [1]. At the microscale, paradigmatic examples include cell aggregates and microorganisms, where motility underlies numerous critical biological processes such as infection and biofilm formation by bacteria, cancer metastasis, tissue repair and wound healing, and complex morphogenesis of new tissues and organs [2–4]. Research on these processes has already provided substantial insight into the biological and physicochemical mechanisms that engender and regulate cellular motility in open uniform domains. However, cells often inhabit complex and heterogeneous three-dimensional environments, such as gels and tissues in the body or soils and sediments in the environment, that impose additional geometric constraints, mechanical cues, and external stimuli such as chemical gradients and fluid flows. These factors fundamentally alter cellular motility, hindering or promoting active transport in unexpected ways and giving rise to fascinating behaviors such as directed cell migration and large-scale coordination [5,6].

Current research efforts in this area aim to expand our understanding of the dynamics of active matter under these constraints to incorporate the complexity of confined, crowded, and structured environments [7]. In many cases, such complex environments challenge preconceived ideas based on studies of either active matter in uniform domains or passive (thermally equilibrated) matter in complex environments. Examples include persistent directional motion in a structured environment under external (e.g., chemotactic) cues [8], the effect of disordered fluid flows [9], coordinated cell migration [10,11], or cell hopping and trapping through porous media [12]. Further progress will stem from the use of accessible experimental realizations.

Using the model unicellular eukaryote *Chlamydomonas reinhardtii* (CR) [13–15], here we present experimental and numerical work that captures the essential features of active particles escaping confinement through narrow apertures, a key component of any structured environment representing the minimal "bridge unit" that connects isolated spatial components or microdomains. For motile bacteria, dynamics through narrow channels gives rise to bistable density oscillations and stable along-axis swimming [16,17]. For microalgae, the escape dynamics through narrow apertures resembles an out-of-equilibrium version of the classical Brownian narrow-escape problem so ubiquitous in physics, chemistry, and biology. This beautiful and mathematically intricate problem, first studied by Lord Rayleigh in the context of acoustics [18], has recently received much attention as the mean escape time controls the rates of fundamental molecular processes (e.g., from mRNA escaping through nucleus pores in the cell [19] to signaling in dendritic spines [20,21]). Instead, for non-Brownian particles following purely ballistic motion, the escape dynamics is captured by the theory of leaking chaotic systems [22], with an exponential decay in particle number only expected for chaotic dynamics, while so-called deterministic billiards give rise to a $1/t$ decay [23–25].

---

*These authors contributed equally to this work.

†ituval@imedea.uib-csic.es
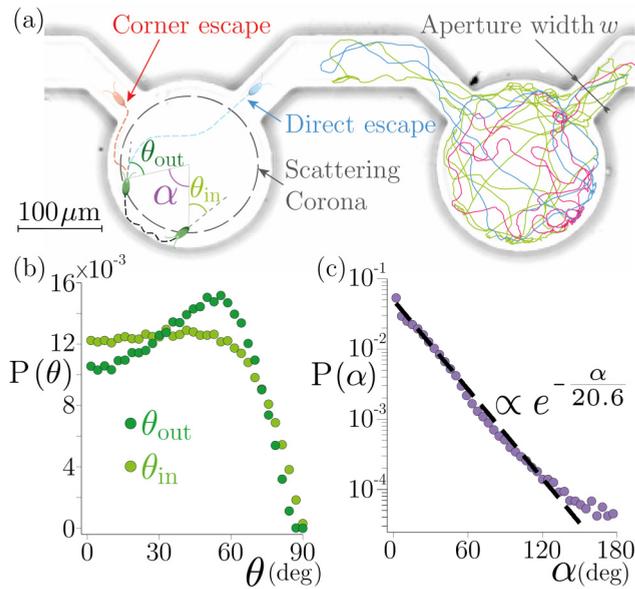
‡mpolin@imedea.uib-csic.es

FIG. 1. Tracking of CR escape through narrow apertures. (a) Left pool: schematic of corner and direct escapes. Right pool: typical trajectories of $N = 3$ algae traveling through and escaping a pool of aperture width w. (b) Distribution of θ_{in} and θ_{out} (obtained over $\sim 2.4 \times 10^5$ events). (c) Distribution of sliding angle α (obtained over $\sim 2 \times 10^5$ events). The fit is an exponential function with a characteristic angle $\bar{\alpha} = 20.6°$.

FIG. 2. Traveled distance in the pool. (a) The distribution of traveled distances ℓ exponentially decays with a characteristic length ℓ_c. Results are shown here for three different aperture widths, with the corresponding exponential fits (lines). (b) The characteristic length ℓ_c inversely decays with the aperture width. Simulations display the same tendency for various values of p_0, the probability to escape after sliding.

Here, we experimentally realize a minimal version of the narrow-escape problem in the context of confined active particles. While recent theoretical works have numerically addressed the effect of swimming characteristics (e.g., persistence length as compared to the domain size [26,27]) or the role of collective interactions [28] for the escape dynamics, we instead focus on the relevance of cell-wall interactions for determining the escape rate. While experimental works addressing the mechanisms of scattering and the interactions of swimmers with a cornerlike geometry have been performed [29], here we tackle the contribution of recently described cell sliding on curved surfaces [30–34] and find that it dominates the escape process for aperture sizes comparable to the size of individual cells.

Chlamydomonas reinhardtii wild-type strain CC125 (CR) was grown in tris-acetate-phosphate medium at $21°C$ under periodic fluorescent illumination (14 h/10 h), as previously described [35]. Culture was harvested in the exponential phase (10^6 cells/mL). CR were loaded into a polydimethylsiloxane (PDMS) microfluidic device, previously passivated with a 0.5% w/v Pluronic F-127 solution, made of a set of quasi-two-dimensional cylindrical pools of radius $R_{pool} \sim 100\,\mu m$ and height $h \sim 20\,\mu m$ interconnected by narrow channels of different aperture sizes w, in the range of 10 to 75 μm [Fig. 1(a)]. Each pool presents two exits located on the pool perimeter at an angular distance of $90°$ from each other. Cells were recorded at 20 fps, with a spatial resolution of $1.85\,\mu m$/pixel to gather accurate statistics on algae escape trajectories over long periods of time (up to tens of minutes). Tracking was performed using an in-house developed Kalman filter-based algorithm, particularly efficient for tracking relatively dense flow of moving objects [36,37].
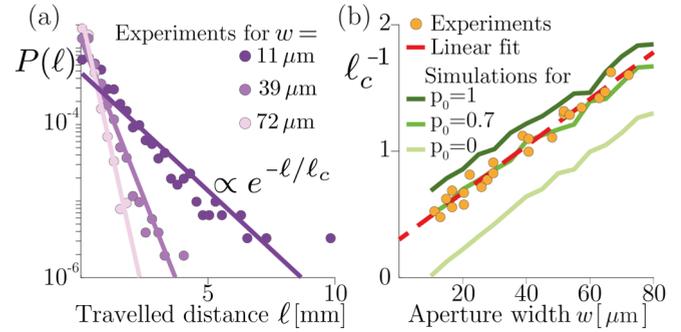
Typical algae trajectories are shown in Fig. 1(a) (and in the Supplemental Material movies showing single-cell tracking [38]) from which we fully characterize free motility parameters in the bulk (pool including the corona): rotational diffusivity, $D_\theta = 1.1\,\text{rad}^2\,\text{s}^{-1}$ and swimming velocity, $v = 70 \pm 50\,\mu m\,\text{s}^{-1}$ (Fig. S1, Supplemental Material [38]). It is apparent that cells strongly interact with pool boundaries and tend to transiently swim aligned to the pool walls when sufficiently close to them. This interaction is reflected in a net accumulation of algae inside a narrow ($\sim 17\,\mu m$ wide) annulus close to the chamber walls [32]. Following [30], we call this interaction area the "scattering corona." and its width approximately corresponds to the cell body size ($a \sim 5\,\mu m$) extended by flagella length ($\ell_{flagella} = 12\,\mu m$). Cell-wall interactions can be simply described by the incoming and outgoing angle distributions with respect to a direction orthogonal to the wall (θ_{in} and θ_{out}, respectively) when entering or exiting the scattering corona. The distribution of θ_{in} is rather constant up to $\theta_{in} \simeq 60°$, and sharply decreases to zero when cells arrive tangentially to the corona [Fig. 1(b)]. The distribution of θ_{out} peaks at about $60°$, which implies that cells tend to exit the corona with a preferred angle after interacting with the wall. In between these two events, cells slide along the pool wall for an angular extent, α, well approximated by a simple exponential distribution [Fig. 1(c)]. As a consequence, we will heuristically describe wall sliding as a Poisson process with a characteristic angle $\bar{\alpha} \simeq 20.6°$.

Turning to the characterization of the narrow-escape process, we select trajectories for which individual cells can be followed for the complete duration of trapping events, i.e., from the time they enter a pool through the connecting channels until the time of escape. The measured persistence length of individual trajectories, $\ell_P = v/D_\theta \simeq 65\,\mu m \lesssim R_{pool}$, places the dynamics close to the crossover to the diffusive regime described in [27]. For all aperture sizes considered, the traveled distance in the pool before escaping is exponentially distributed [Fig. 2(a)], as expected for leaking chaotic billiards, with the characteristic length ℓ_c inversely proportional to the aperture size [dots, Fig. 2(b)]—cells travel a larger distance before escaping when trapped in pools

TABLE I. List of parameters used for the simulations.

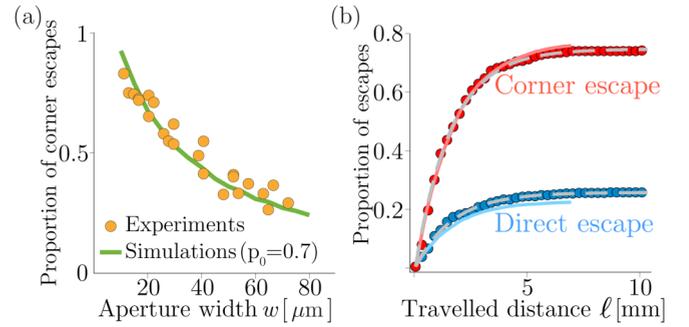| Parameter	Value
Radius of the pool	$R_{\text{pool}} = 101.6\,\mu\text{m}$
Radius of the swimmer	$a = 3.8\,\mu\text{m}$
Velocity of the swimmer	$v = 70\,\mu\text{m s}^{-1}$
Rotational diffusion	$D_\theta = 1.1\ \text{rad}^2\,\text{s}^{-1}$
Sliding angle	$\bar{\alpha} = 20.6\,^\circ$
Scattering angle	$\theta_{\text{out}} = 41.5\,^\circ$
Time step	$\Delta t = 0.1\,\text{s}$
No. cells	$N_{\text{cells}} = 10^3$
No. steps	$N_{\text{steps}} = 10^4$

FIG. 3. Corner escapes. (a) Ratio of corner escapes relative to the total number of escapes, $n_c^\infty/(n_c^\infty + n_d^\infty)$, as a function of the aperture width w. (b) Proportion of direct $[n_d(\ell)/(n_c^\infty + n_d^\infty)]$ and corner $[n_c(\ell)/(n_c^\infty + n_d^\infty)]$ escapes as a function of the traveled distance ℓ within a pool for experiments (filled circles) and simulations (lines, for $p_0 = 0.7$). Data are shown for an aperture width $w = 15\ \mu\text{m}$. The dashed lines represent experimental data fitted with a model of type $A(1 - e^{-B\ell})$.

connected by narrower channels. This exponential fit confirms that the difference for escape dynamics between cells derives from variability in swimming velocity. Strikingly, a linear fit to ℓ_c^{-1} shows that this trend leads to a significant escape rate even for the case $w = 2a$ ($\ell_c^{-1} = 0.47 \pm 0.07\,\mu\text{m}^{-1}$), where it would be natural to expect instead a divergence of the mean escape time. This hints at the existence of an additional mechanism facilitating escapes as yet overlooked.

Indeed, a careful reexamination of all recorded escape events shows that these can be categorized into two distinct classes: *direct escapes*, in which cells directly swim towards the aperture from bulk after a last scattering with distant walls, and *corner escapes*, where cells slide along the curved walls to reach the aperture and eventually leave the pool without leaving the scattering corona [Fig. 1(a)]. We further explore the relevance of this categorization by building a minimal model of the escape process as follows: we simulate N_{cell} noninteracting circular swimmers of radius a confined to a two-dimensional circular pool of radius R_{pool} with two openings of width w set at 90° apart. The cells' position and orientation are randomly initialized with all parameters (e.g., swimming speed v and rotational diffusivity D_θ) extracted from our experimental data and summarized in Table I. At each time step of the simulation, the velocity of swimmers is constant and a random reorientation $\delta\theta$ of swimmers is considered, defined thanks to the rotational diffusivity D_θ. Over the course of a numerical simulation, if the cell reaches an aperture without touching the wall, then it directly escapes the pool. However, if the finite-size swimmer enters in contact with the pool boundary, it slides for a sliding angle α randomly picked from the experimentally measured exponential distribution [Fig. 1(c) and Table I]. If a cell slides for a distance greater than that needed to reach the closest aperture, it escapes the pool with a probability p_0 through a corner escape. Otherwise, it remains in the pool and it is scattered back from the corona towards the bulk with an angle θ_{out} corresponding to the mean experimental scattering angle (see Supplemental Material [38]). Using instead the peak value for θ_{out} or drawing the angle from the full experimental distribution only has a minor quantitative effect on the presented results (Figs. S2 and S3, Supplemental Material [38]).

This approach qualitatively reproduces the experimentally observed exponential distributions for ℓ as well as the decay of the characteristic traveled distance ℓ_c with w [Fig. 2(b)]. While for $p_0 = 0$, i.e., in the absence of *corner* escapes, the

average traveled distance in the pool is significantly higher than that observed in experiments and indeed ℓ_c diverges ($\ell_c^{-1} \to 0$ for $w \to a$), we find that $p_0 = 0.70$ best matches our experimental data. Hence, we unambiguously report that cells are biased in their trajectory by the presence of curved walls, with CR repeatedly sliding along the wall towards the exit to escape. Figure 3(a) shows how the ratio of corner escapes (n_c^∞ at the end of the experiment) over the total number of escapes ($n_c^\infty + n_d^\infty$ at the end of the experiment) depends on the size of the aperture, with corner escapes accounting for $\sim 90\%$ of total events for the smallest w. As an independent verification, our minimal numerical model, where $p_0 = 0.70$ is the sole fitting parameter, matches the experimentally measured values well [Figs. 3(a) and 3(b)].

Can we separate the narrow-escape dynamics into two distinct independent—additive—processes, i.e., *corner* and *direct escapes*? Under this assumption they would be characterized by different escape rates, λ_c and λ_d, respectively, leading to a simple balance of escape types:

$$\frac{dn_c}{d\ell} = \lambda_c(1 - n_t), \qquad \frac{dn_d}{d\ell} = \lambda_d(1 - n_t),$$

$$\frac{dn_t}{d\ell} = \lambda_t(1 - n_t) = (\lambda_c + \lambda_d)(1 - n_t), \qquad (1)$$

where $n_c(\ell)$, $n_d(\ell)$, and $n_t(\ell)$ denote the normalized number of corner, direct, and total escapes, and λ_t the total escape rate. The solutions to these three equations were independently fitted to the experimental data (and compared with the results of simulations) to extract the values of the various escape rates λ involved, as shown in Fig. 3(b) for $w = 15\ \mu\text{m}$.

For all explored w, the rate of total escapes λ_t simply equals the sum of λ_c and λ_d [Fig. 4(a)]. Moreover, we observe an excellent agreement between experimental (dots) and numerical (lines) results. In particular, the rate of corner escapes is constant over all aperture sizes, while the rate of direct escapes increases linearly, as expected from simple geometric arguments for the likelihood that a hit on the boundary happens where the exit is if swimmers scatter off walls with fixed scattering angle θ_{out}. Consequently, the proportion of
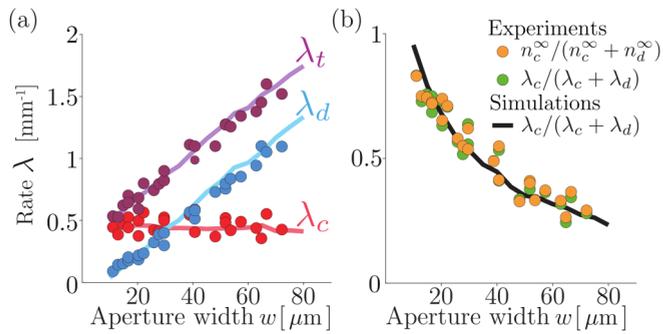
FIG. 4. Escape rates are additive. (a) Corner (λ_c), direct (λ_d), and total (λ_t) escape rates for various aperture sizes, from experimental (dots) and simulation (lines). The exponential fits to estimate these rates give a mean reduced χ_ν^2 of 1.05, 0.87, and 1.26 (1.00, 0.95, and 0.70) for corner, direct, and total escapes from experiment (simulation). All values are available in Table S1, Supplemental Material [38]. (b) Comparison between the experimental proportion of corner escapes $n_c^\infty/(n_c^\infty + n_d^\infty)$ [same as from Fig. 3(a)] and the ratios $\lambda_c/(\lambda_c + \lambda_d)$ issued from both experiments and simulations (for $p_0 = 0.7$).

corner escapes [shown in Fig. 3(a)] could simply be understood as the ratio $\lambda_c/(\lambda_c + \lambda_d)$ as confirmed in Fig. 4(b) and which is, once again, well captured by our numerical results.

We present an experimental study of the narrow-escape problem for microswimmers in circular pools. We find that for pools of size comparable to the cells' persistence length

($\ell_P \simeq 65\,\mu$m), the escape dynamics is well captured by a weakly stochastic billiard with particles scattering off walls at fixed outgoing angles. We demonstrate that a crucial role is played by the hydrodynamic and steric forces that cause swimming cells to adhere to the pool walls and slide, guiding them to and through the exit. This results in two escape mechanisms with very distinctive trends that when combined, elicit a significantly faster escape from confinement in a broad range of swimming parameters. The importance of boundary interactions for the escape through exits close to the active particles' size points to the importance to further investigate the effect of microdomain geometry in the immediate vicinity of narrow channels and the effect this has on microswimmers' dynamics. Finally, our work is neatly supported by numerical simulations that recapitulate our experimental observations. Altogether, these highlight the significance of considering the details of cell-wall interactions for the narrow-escape problem of active particles.

[1] M. C. Marchetti, J. F. Joanny, S. Ramaswamy, T. B. Liverpool, J. Prost, M. Rao, and R. A. Simha, Hydrodynamics of soft active matter, Rev. Mod. Phys. **85**, 1143 (2013).

[2] R. Hartmann, P. K. Singh, P. Pearce, R. Mok, B. Song, F. Díaz-Pascual, J. Dunkel, and K. Drescher, Emergence of three-dimensional order and structure in growing biofilms, Nat. Phys. **15**, 251 (2019).

[3] D. Needleman and Z. Dogic, Active matter at the interface between materials science and cell biology, *Nature Reviews Materials* (Nature Publishing Group, 2019), Vol. 2, pp. 1–14.

[4] C. Collinet and T. Lecuit, Programmed and self-organized flow of information during morphogenesis, *Nature Reviews Molecular Cell Biology* (Nature Publishing Group, 2021), Vol. 22, pp. 245–265.

[5] A. Bricard, J.-B. Caussin, N. Desreumaux, O. Dauchot, and D. Bartolo, Emergence of macroscopic directed motion in populations of motile colloids, Nature **503**, 95 (2013).

[6] M. Rein, N. Heinß, F. Schmid, and T. Speck, Collective Behavior of Quorum-Sensing Run-and-Tumble Particles under Confinement, Phys. Rev. Lett. **116**, 058102 (2016).

[7] C. Bechinger, R. Di Leonardo, H. Löwen, C. Reichhardt, G. Volpe, and G. Volpe, Active particles in complex and crowded environments, Rev. Mod. Phys. **88**, 045006 (2016).

[8] T. V. Phan, R. Morris, M. E. Black, T. K. Do, K.-C. Lin, K. Nagy, J. C. Sturm, J. Bos, and R. H. Austin, Bacterial Route Finding and Collective Escape in Mazes and Fractals, Phys. Rev. X **10**, 031017 (2020).

[9] P. de Anna, A. A. Pahlavan, Y. Yawata, R. Stocker, and R. Juanes, Chemotaxis under flow disorder shapes microbial dispersion in porous media, Nat. Phys. **17**, 68 (2021).

[10] D. B. Brückner, N. Arlt, A. Fink, P. Ronceray, J. O. Rädler, and C. P. Broedersz, Learning the dynamics of cellcell interactions in confined cell migration, Proc. Nat. Acad. Sci. USA **118**, 7 (2021).

[11] J. Renkawitz, A. Kopf, J. Stopp, I. de Vries, M. K. Driscoll, J. Merrin, R. Hauschild, E. S. Welf, G. Danuser, R. Fiolka *et al.*, Nuclear positioning facilitates amoeboid migration along the path of least resistance, Nature (London) **568**, 546 (2019).

[12] T. Bhattacharjee and S. S. Datta, Confinement and activity regulate bacterial motion in porous media, Soft Matter **15**, 9920 (2019).

[13] E. H. Harris, Chlamydomonas as a model organism, Annu. Rev. Plant. Physiol. Plant. Mol. Biol. **52**, 363 (2001).

[14] E. H. Harris, *The Chlamydomonas Sourcebook* (Elsevier, Amsterdam, 2009).

[15] R. E. Goldstein, Green Algae as model organisms for biological fluid dynamics, Annu. Rev. Fluid Mech. **47**, 343 (2015).

[16] M. Paoluzzi, R. Di Leonardo, and L. Angelani, Self-sustained density oscillations of swimming bacteria confined in microchambers, Phys. Rev. Lett. **115**, 188303 (2015).

[17] G. Vizsnyiczai, G. Frangipane, S. Bianchi, F. Saglimbeni, D. Dell'Arciprete, and R. Di Leonardo, A transition to stable one-dimensional swimming enhances E. coli motility through narrow channels, Nat. Commun. **11**, 2340 (2020).

[18] J. W. S. B. Rayleigh, *The Theory of Sound*, Vol. 2 (Macmillan, London, 1878).

[19] O. G. Berg, R. B. Winter, and P. H. von Hippel, Diffusion-driven mechanisms of protein translocation on nucleic acids. 1. Models and theory, Biochemistry **20**, 6929 (1981).

[20] K. M. Harris and J. K. Stevens, Dendritic spines of rat cerebellar Purkinje cells: Serial electron microscopy with reference to their biophysical characteristics, J. Neurosci. **8**, 4455 (1988).

[21] D. Holcman, E. Korkotian, and M. Segal, Calcium dynamics in dendritic spines, modeling and experiments, Cell Calcium **37**, 467 (2005).

[22] E. G. Altmann, J. S. E. Portela, and T. Tél, Leaking chaotic systems, Rev. Mod. Phys. **85**, 869 (2013).

[23] W. Bauer and G. F. Bertsch, Decay of Ordered and Chaotic Systems, Phys. Rev. Lett. **65**, 2213 (1990).

[24] M. S. Krieger, Microorganism billiards in closed plane curves, Eur. Phys. J. E **39**, 122 (2016).

[25] S. E. Spagnolie, C. Wahl, J. Lukasik, and J. L. Thiffeault, Microorganism billiards, Physica D **341**, 33 (2017).

[26] L. Caprini, F. Cecconi, and U. Marini Bettolo Marconi, Transport of active particles in an open-wedge channel, J. Chem. Phys. **150**, 144903 (2019).

[27] M. Paoluzzi, L. Angelani, and A. Puglisi, Narrow-escape time and sorting of active particles in circular domains, Phys. Rev. E **102**, 042617 (2020).

[28] K. S. Olsen, L. Angheluta, and E. G. Flekkøy, Escape problem for active particles confined to a disk, Phys. Rev. Research **2**, 043314 (2020).

[29] V. Kantsler, J. Dunkel, M. Polin, and R. E. Goldstein, Ciliary contact interactions dominate surface scattering of swimming eukaryotes, Proc. Natl. Acad. Sci. USA **110**, 1187 (2013).

[30] M. Contino, E. Lushi, I. Tuval, V. Kantsler, and M. Polin, Microalgae Scatter off Solid Surfaces by Hydrodynamic and Contact Forces, Phys. Rev. Lett. **115**, 258102 (2015).

[31] O. Sipos, K. Nagy, R. Di Leonardo, and P. Galajda, Hydrodynamic Trapping of Swimming Bacteria by Convex Walls, Phys. Rev. Lett. **114**, 258104 (2015).

[32] T. Ostapenko, F. J. Schwarzendahl, T. J. Böddeker, C. T. Kreis, J. Cammann, M. G. Mazza, and O. Bäumchen, Curvature-Guided Motility of Microalgae in Geometric Confinement, Phys. Rev. Lett. **120**, 068002 (2018).

[33] A. Théry, Y. Wang, M. Dvoriashyna, C. Eloy, F. Elias, and E. Lauga, Rebound and scattering of motile: Chlamydomonas algae in confined chambers, Soft Matter **17**, 4857 (2021).

[34] J. Cammann, F. J. Schwarzendahl, T. Ostapenko, D. Lavrentovich, O. Bäumchen, and M. G. Mazza, Emergent probability fluxes in confined microbial navigation, Proc. Natl. Acad. Sci. USA **118**, e2024752118 (2021).

[35] A. J. T. M. Mathijssen, R. Jeanneret, and M. Polin, Universal entrainment mechanism controls contact times with motile cells, Phys. Rev. Fluids **3**, 033103 (2018).

[36] R. E. Kalman, A new approach to linear filtering and prediction problems, J. Basic Eng. **82**, 35 (1960).

[37] M. Souzy, I. Zuriguel, and A. Marin, Transition from clogging to continuous flow in constricted particle suspensions, Phys. Rev. E **101**, 060901(R) (2020).

[38] See Supplemental Material at http://link.aps.org/supplemental/10.1103/PhysRevResearch.4.L022029 doi for the following: (i) a movie of algae moving through a network of pools interconnected by channels; the movie highlights two portions of distinct algae trajectories detected by the particle tracking algorithm, which illustrate a corner and a direct escape from a pool; (ii) a movie highlighting the detected track of an alga, and its trace; (iii) figures that display the distribution of cell velocity (Fig. S1), the traveled distance in the pool from simulation using the peak value for θ_{out} (Fig. S2) and using the full experimental distribution (Fig. S3), and a table recapitulating the goodness of fit to derive escape rates (Table S1); and (iv) the simulation codes and simulation results used throughout the Letter.